NeuroImage 300 (2024) 120860

Contents lists available at ScienceDirect

NeuroImage

journal homepage: www.elsevier.com/locate/ynimg

Astroglial glucose uptake determines brain FDG-PET alterations and metabolic connectivity during healthy aging in mice

Laura M. Bartos [a], Sebastian T. Kunte [a], Stephan Wagner [a], Philipp Beumers [a], Rebecca Schaefer [a], Artem Zatcepin [a,b], Yunlei Li [a], Maria Griessl [a], Leonie Hoermann [a], Karin Wind-Mark [a,b], Peter Bartenstein [a,c], Sabina Tahirovic [b], Sibylle Ziegler [a,c], Matthias Brendel [a,b,c], Johannes Gnörich [a,b,*]

[a] Department of Nuclear Medicine, LMU University Hospital, LMU Munich, Munich, Germany
[b] German Center for Neurodegenerative Diseases (DZNE) Munich, Germany
[c] Munich Cluster for Systems Neurology (SyNergy), Munich, Germany

ARTICLE INFO

Keywords:
FDG-PET
Aging
Astroglia
Metabolic connectivity
Scradiotracing

ABSTRACT

Purpose: 2-Fluorodeoxyglucose-PET (FDG-PET) is a powerful tool to study glucose metabolism in mammalian brains, but cellular sources of glucose uptake and metabolic connectivity during aging are not yet understood.
Methods: Healthy wild-type mice of both sexes (2–21 months of age) received FDG-PET and cell sorting after in vivo tracer injection (scRadiotracing). FDG uptake per cell was quantified in isolated microglia, astrocytes and neurons. Cerebral FDG uptake and metabolic connectivity were determined by PET. A subset of mice received measurement of blood glucose levels to study associations with cellular FDG uptake during aging.
Results: Cerebral FDG-PET signals in healthy mice increased linearly with age. Cellular FDG uptake of neurons increased between 2 and 12 months of age, followed by a strong decrease towards late ages. Contrarily, FDG uptake in microglia and astrocytes exhibited a U-shaped function with respect to age, comprising the predominant cellular source of higher cerebral FDG uptake in the later stages. Metabolic connectivity was closely associated with the ratio of glucose uptake in astroglial cells relative to neurons. Cellular FDG uptake was not associated with blood glucose levels and increasing FDG brain uptake as a function of age was still observed after adjusting for blood glucose levels.
Conclusion: Trajectories of astroglial glucose uptake drive brain FDG-PET alterations and metabolic connectivity during aging.

1. Introduction

2-Fluorodeoxyglucose positron emission tomography (FDG-PET) is frequently used to study glucose metabolism in mammalian brains and acts as a valuable biomarker in distinguishing between physiological aging and neurodegenerative conditions in dementias (Bohnen et al., 2012). Assessment of glucose metabolism in rodent brains via FDG-PET has been established in the last couple of decades and provides the unique opportunity to enhance the understanding of human pathophysiology via back-translation. This is particularly important since several studies highlighted the direct relevance of astrocytic (Zimmer et al., 2017; Rocha et al., 2022) and microglial (Xiang et al., 2021) FDG uptake to FDG-PET signals. Furthermore, our recent study revealed a strong contribution of microglia to metabolic connectivity in the rodent brain (Gnörich et al., 2023), which acts as a comprehensive readout of regionally synchronized glucose metabolism (S. Morbelli et al., 2013). However, cellular FDG uptake and metabolic connectivity of the rodent brain have not yet been investigated during aging and contributions of different cells to the total FDG-PET signal remain to be elucidated.

Thus, we aimed to decipher the underlying cellular sources of FDG-PET signal changes during aging and their impact on the metabolic connectome of the rodent brain. We used an integrated concept of FDG-PET imaging and cell sorting after in vivo FDG injection (scRadiotracing) to determine the differential contributions of astroglia and neurons to FDG-PET signals and metabolic connectivity as a function of age.

* Corresponding author at: Marchinonistrasse 15, 81377 Munich, Germany
E-mail address: Johannes.Gnoerich@med.uni-muenchen.de (J. Gnörich).

https://doi.org/10.1016/j.neuroimage.2024.120860
Received 16 July 2024; Received in revised form 24 August 2024; Accepted 18 September 2024
Available online 25 September 2024

2. Materials and methods

2.1. Experimental setup and study design

FDG-PET scans, determination and calculation of single cell FDG uptake after in vivo tracer injection (scRadiotracing (Bartos et al., 2022)) and measurements of blood glucose levels were acquired under harmonized conditions. A detailed overview of the study groups is provided in Table 1. Sample sizes for analyses of FDG-PET and metabolic connectivity were based on published data (Ruch et al., 2024). No randomisation was used to allocate experimental units due to absence of intervention. Pseudo-blinding was achieved by operator independent quantification. The experiments were approved by the local animal care committee of the Government of Oberbayern and were overseen by a veterinarian in compliance with the Animal Research: Reporting In Vivo Experiments (ARRIVE) guidelines (**Supplement**) as well as the EU Directive 2010/63/EU for animal experiments. All C57BL/6 J wild-type mice included in this study were acquired commercially (JAX® Mice Strain, Charles River, The Jackson Laboratory). Animals were housed in a controlled environment with regulated temperature and humidity, maintained under a 12-hour light-dark cycle, and were provided with free access to food (Ssniff Spezialdiäten GmbH, Soest, Germany) and water. Anesthesia was induced before FDG application and maintained during the PET scan with 1.5 % isoflurane delivered via a mask at 3.5 L/min.

2.2. FDG-PET image acquisition, preprocessing and analysis

Cross-sectional rodent FDG-PET procedures in $n = 197$ wild-type mice followed an established standardized protocol for radiochemistry, acquisition times, and post-processing (Brendel et al., 2016). In brief, static FDG emission recording was performed for 30 min (30–60 min p.i.) using a Siemens Inveon small animal PET. In an additional cohort, FDG-PET images of $n = 27$ wild-type mice were obtained from a MedisonanoScan PET/CT system consistently using 30–45 min p. i. as static analysis window. Due to different PET scanner systems, PET imaging data of both cohorts were not pooled. One wild-type mouse of the second cohort died during FDG-PET scan and was therefore excluded for further analysis. FDG-PET preprocessing for all image data was performed by PMOD V3.5 (PMOD technologies, Basel, Switzerland). Unified spatial normalization (nonlinear warping, transient 0.6 mm^3 Gaussian smoothing of the input image, 16 iterations, frequency cutoff 3, no thresholding) of all original FDG-PET images to the same previously established FDG-PET template was performed, to ensure spatial comparability between all different studies. Volumes of interest (VOIs) were defined on a T1 MRI template in Ma-Benveniste-Mirrione atlas space including anatomical compartments and functional subdivision (Ma et al., 2005). Standardized uptake values (SUVs; 30–60 or 30–45 min p.i.) in VOIs were calculated by scaling to the injected dose and normalizing for body weight (tracer uptake in VOI/(injected activity/-mouse weight)). Additionally, whole brain SUV was determined per individual mouse. For FDG-PET SUV analyses, we only included animals for which successful intravenous tracer injection could be assumed (total of $n = 155$) to ensure unbiased SUV values, since we had enough samples to ensure high statistical power. In these animals, back-measurement of the syringe should be <30 % of the initial radioacitivity in the syringe before tracer application. Animals with back-measurement above 30 % ($n = 42$) were only used for analyses using in-brain normalization variants, which are less susceptible to limited amounts of paravenous tracer injection. Adjusted SUV were calculated under consideration of blood glucose levels in $n = 27$ individual mice as a surrogate measure of cerebral metabolic rate of glucose (MRglc) (Bertoglio et al., 2021) (SUVglc = SUVmax*blood glucose /100 mg/dl).

Table 1
Summary of analyzed data.

Age (months)	Animal (n)	Modality	Sex (f/m)	Weight (g)	Injected dose (MBq)
2–3	16	PET	8/8	23.5 ± 2.2	14.8 ± 1.9
2–3	6	scRadiotracing	4/2	24.2 ± 3.1	17.8 ± 1.7
2–4	9	scRadiotracing + blood glucose assessment	2/7	24.1 ± 3.5	29.4 ± 2.2
5	37	PET	15/22	28.0 ± 2.9	14.4 ± 1.7
6	33	PET	28/5	25.5 ± 3.4	14.3 ± 1.5
6	6	scRadiotracing	6/0	22.5 ± 2.5	33.7 ± 10.2
8	21	PET	16/5	25.6 ± 3.0	14.4 ± 1.5
8–13	11	scRadiotracing + blood glucose assessment	2/9	28.8 ± 3.8	28.4 ± 2.8
10	25	PET	23/2	24.6 ± 1.8	13.9 ± 1.9
12	18	PET	15/3	33.2 ± 3.7	15.4 ± 1.5
12	10	scRadiotracing	7/3	29.8 ± 3.1	20.3 ± 5.3
14	17	PET	17/0	29.8 ± 3.4	15.2 ± 2.7
16	18	PET	18/0	32.0 ± 3.2	15.2 ± 3.2
17–21	7	scRadiotracing + blood glucose assessment	2/5	35.9 ± 4.0	28.0 ± 1.6
18	12	PET	8/4	32.6 ± 1.7	14.1 ± 2.8
18	5	scRadiotracing	1/4	35.3 ± 2.1	27.7 ± 2.9

2.3. Correlation and connectivity analyses

Metabolic connectivity patterns were derived in $n = 197$ wild-type mice as previously described (Gnörich et al., 2023). In brief, 21 brain regions were defined based on the anatomical correlates outlined in the Ma-Benveniste-Mirrione atlas, with slight modifications according to our previous work (Gnörich et al., 2023; Ruch et al., 2024). After global mean scaling, we performed inter-regional correlation resulting in 21 × 21 individual Pearson's correlation coefficient pairs (with subsequent Fisher z-transformation) of which 8 × 8 belonged to cortical networks and 13 × 13 belonged to subcortical networks (**Supplemental Figure 1**). Average interregional correlation coefficients (ICCs) were then calculated by taking the mean across the composite of functional regions (e.g. intra-cortical) for each age group. To illustrate the most significant ICCs within each group of mice, we utilized a specially designed Python script built on Matplotlib and Scikit-image. We projected the centers of VOIs onto a 3D mouse brain template, focusing on those with ICC values surpassing a defined threshold (0.5). These selected VOIs were then depicted as nodes, where the size of each node corresponds to the count of ICCs above the specified threshold for the respective VOI. Additionally, connection lines between nodes visually represent the ICC values between the corresponding VOIs.

2.4. scRadiotracing

ScRadiotracing (Bartos et al., 2022) was performed on a total of $n = 54$ wild-type mice as described previously. This group of animals consisted of two separate cohorts. The first cohort ($n = 27$) received scRadiotracing only. In the second cohort ($n = 27$), FDG-PET imaging and blood glucose measurement were performed prior to scRadiotracing. One wild-type mouse of the second cohort died during FDG-PET scan and was therefore excluded for further analyses. Detailed descriptions of

brain dissociation and cell isolation are provided in the **Supplement**. In brief, brains were removed 45–50 min after FDG injection, whole brain activity was measured, scaled to the injected dose and normalized for body weight. This procedure was followed by enzymatic dissociation into a single cell suspension. After debris and red blood cell removal, astrocytes, microglia and neurons were isolated via fluorescence activated cell sorting. FDG uptake per single cell was calculated after determination of the cell count via flow cytometry and determination of the radioactivity in a gamma counter. In $n = 14$ mice of the first cohort ($n = 27$ mice without FDG-PET), we successfully determined FDG uptake in all three cell types, when using a signal-to-noise threshold of ≥ 2 (relative to the empty vial). Subsequently, the ratio between summed uptake in astrocytes and microglia versus the uptake in neurons was calculated as FDG Glia-to-Neuron ratio. Samples which showed a signal-to-noise ratio < 2 after scRadiotracing were excluded.

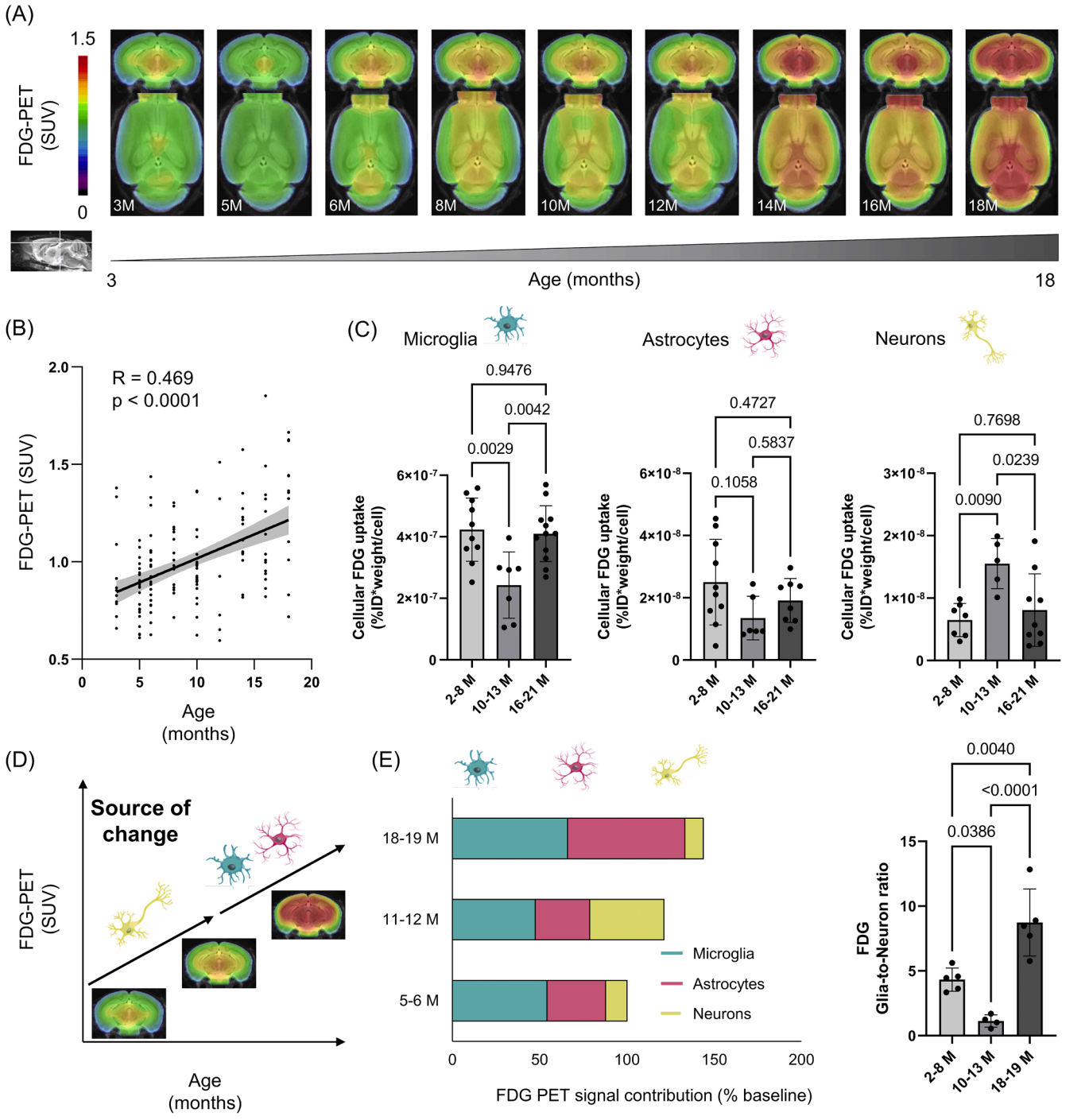

Fig. 1. FDG-PET uptake and cellular glucose allocation during aging in wild-type mice. (A) Axial and coronal FDG-PET images at different ages upon an MRI template. (B) Linear regression of FDG-PET SUV as a function of age for the whole brain. (C) Single cell FDG uptake of microglia, astrocytes and neurons in comparison of three time-points (6/12/18 months), normalized by injected dose and body weight. (D) Schematic illustration of cellular contributions to changes of FDG-PET signals with age. (E) Estimated cellular allocation of FDG-PET signals per age, derived from a bootstrapped equation system and ratio of glial to neuronal FDG uptake in comparison in groups with increasing age.

2.5. Statistical analyses

Statistical tests were performed using SPSS (V27.0; IBM Corp.) and GraphPad Prism (V9.5.1; GraphPad Software, LCC). Coefficients of correlation (R) were calculated for the function (Akaike information criterion (AIC) selection of: linear, quadratic, cubic, logarithmic) between age and i) FDG-PET SUV, ii) metabolic connectivity iii) FDG Glia-to-Neuron-ratio. The agreement between age-related functions of metabolic connectivity and the FDG Glia-to-Neuron-ratio was tested by Pearson's correlation. Additionally, the agreement between blood glucose, weight and age as well as whole brain FDG uptake, FDG-PET and single cell FDG uptake of microglia, astrocytes and neurons was examined via Pearson's correlation. One-way ANOVA with Tukey post-hoc correction for multiple comparisons was used to compare cellular FDG uptake, FDG Glia-to-Neuron-ratio whole brain FDG uptake as well as FDG-PET SUV between young (2–8 months of age), intermediate (10–13 months of age) and old (16–21 months of age) mice. The allocation of age-dependent FDG-PET signals to cellular sources was estimated by benchmarking through a linear equation system matrix with three equations (I: young, II: intermediate, III: old) and three unknowns (x: microglial contribution, y: astrocytic contribution, z: neuronal contribution) using whole brain FDG-PET SUV per age realted group as a fixed factor. The equation system was set as follows, with M = microglial FDG uptake (%ID*BW/cell), A = astrocytic FDG uptake (%ID*BW/cell), N = neuronal FDG uptake (%ID*BW/cell):

$$I:\ FDG\ PET\ SUV\ (young) = M(young) * x + A(young) * y + N(young) * z$$

$$II:\ FDG\ PET\ SUV\ (interm.) = M(interm.) * x + A(interm.) * y + N(interm.) * z$$

$$III:\ FDG\ PET\ SUV\ (old) = M(old) * x + A(old) * y + N(old) * z$$

Each possible combination of individual samples using one sample per age related group ($5 \times 4 \times 5$) served for calculation of the average contribution per cell type (average of $n = 100$ calculated equation systems). By additional consideration of the changes of FDG-PET SUV with age and changes in cellular FDG uptake with age, we determined the contribution of each cell type to FDG-PET SUV per age related group, relative to the baseline of young mice.

3. Results

3.1. Neuronal and astroglial contributions to age-related changes in FDG-PET signals

Cerebral FDG-PET signals showed an age-dependent increase of SUV. The AIC calculation suggested that a linear fit was the best of the tested models for describing the association of cerebral FDG-PET SUV and age ($R = 0.469$, $F_{(2153)} = 43.2$, $p < 0.0001$, Fig. 1A,B). Microglia (−28 %, $p = 0.0034$) and astrocytes (−46 %, $p = 0.117$) showed a decrease of FDG uptake from young to intermediate ages, followed by a recovery of FDG uptake per astroglial cell in mice at late ages (microglia: +39 %, $p = 0.0042$; astrocytes: +42 %, $p = 0.584$; Fig. 1C). Contrarily, FDG uptake of neurons indicated a distinct increase of glucose uptake from young to intermediate ages (+140 %, $p = 0.0090$), followed by a subsequent strong decrease of cellular FDG uptake in mice at late ages (−48 %, $p = 0.0239$; Fig. 1C). Thus, neuronal FDG uptake explained the increase in FDG-PET signals from young to intermediate ages, whereas the FDG-PET signal increase from intermediate to late ages was explained by astroglial FDG uptake (Fig. 1D). Considering cellular FDG uptake and cell proliferation during healthy aging [12,13], astroglia showed a stronger contribution to FDG-PET signals compared to neurons at all ages studied (65 %–93 %; Fig. 1E). The FDG Glia-to-Neuron-ratio indicated a u-shaped function of age (Fig. 1E).

3.2. Associations between metabolic connectivity and the FDG Glia-to-Neuron-ratio in aging mice

Metabolic connectivity was analyzed in nine groups of wild-type mice with increasing age and showed a decrease of metabolic connectivity in the cortical network from young to intermediate ages, followed by an increase of metabolic connectivity towards late age (Fig. 2A, B). Subcortical metabolic connectivity did not significantly change during aging (Fig. 2A, C). Cortical metabolic connectivity and the FDG Glia-to-Neuron-ratio developed as aligned trajectories over time ($R = 0.900$, $p < 0.0001$). AIC calculation revealed a quadratic regression as the best fit for both read-outs (cortical metabolic connectivity: $R = 0.988$, $F(2,7) = 122.8$, $p < 0.0001$; FDG Glia-to-Neuron-ratio: $R = 0.881$, $F(2,12) = 19.9$, $p = 0.0003$) (Fig. 2D). No agreement was observed between subcortical metabolic connectivity and the FDG Glia-to-Neuron-ratio ($R = 0.129$, $p = 0.489$, Fig. 2E). Further investigation of the interregional cortico-hippocampal network revealed a logarithmic decrease with age ($R = 0.541$, $F(2,7) = 15.6$, $p < 0.0001$), but no association with the FDG-Glia-to-Neuron ratio ($R = 0.089$, $p = 0.633$) (Supplemental Fig. 2).

3.3. Impact of blood glucose levels on whole brain and single cell glucose uptake

Blood glucose ($R = 0.415$, $p = 0.031$) and body weight ($R = 0.815$, $p < 0.0001$) showed a linear increase as a function of age (Fig. 3A). Hence, also blood glucose was positively correlated with body weight ($R = 0.465$, $p = 0.014$, Fig. 3A). In this subset of mice, increasing brain glucose uptake with age was reproduced (Fig. 3B) and the increase of brain glucose uptake at intermediate and late ages was still obvious when adjusting for blood glucose levels (+39 % vs. +82 %, $p = 0.0001$, Fig. 3B). In this regard, brain FDG-PET SUV and ex vivo brain glucose uptake showed a strong agreement (Fig. 3B). Only a slightly negative trend was observed for the association between blood glucose levels and brain glucose uptake ($R = -0.165$, $p = 0.410$, Fig. 3B). In line, no significant associations between blood glucose levels and cellular FDG uptake were observed for microglia ($R = 0.159$, $p = 0.571$), astrocytes ($R = -0.410$, $p = 0.362$) and neurons ($R = -0.194$, $p = 0.525$, Fig. 3C).

4. Discussion

The main finding of this investigation demonstrates that astroglial FDG uptake dominates the cellular allocation of FDG-PET signals and FDG-PET changes during aging in healthy mice. Furthermore, we propose a Glia-to-Neuron-ratio of cellular FDG uptake, which closely correlates with cortical metabolic connectivity.

We performed a comprehensive analysis of small-animal FDG-PET in 224 wild-type mice imaged between 2 and 21 months of age in which we observed a continuous increase in brain glucose metabolism with aging. Likewise, previous small-animal PET studies reported an increase of cortical FDG uptake as a function of age in wild-type mice up to 14–15 months of age (Poisnel et al., 2012; Brendel et al., 2017) and 19 months of age (de Cristobal et al., 2014). On the contrary, several human studies reported decreasing brain FDG-PET signals during aging (Kalpouzos et al., 2009; Kakimoto et al., 2016). This effect may arise from different life expectancy, since rodent brains at the age of 16 months reflect a human age of approximately 40–50 years, when declining cerebral energy metabolism becomes first evident (Kakimoto et al., 2016).

Still, the evident increase of FDG-PET signals with aging in mice allowed us to determine the underlying cellular sources of changes in FDG-PET signals by an integrated analysis of PET and scRadiotracing (Bartos et al., 2022). Here, we observed a clear reduction of cellular FDG uptake in neurons in mice at late ages, whereas astroglia showed an increase in FDG uptake compared to 10–13 months of age. This clearly indicated that increasing FDG-PET signals in the rodent brain towards late ages are driven by astroglial activation, which fits to spatial coupling of FDG- and TSPO-PET signal increases (Focke et al., 2019). In

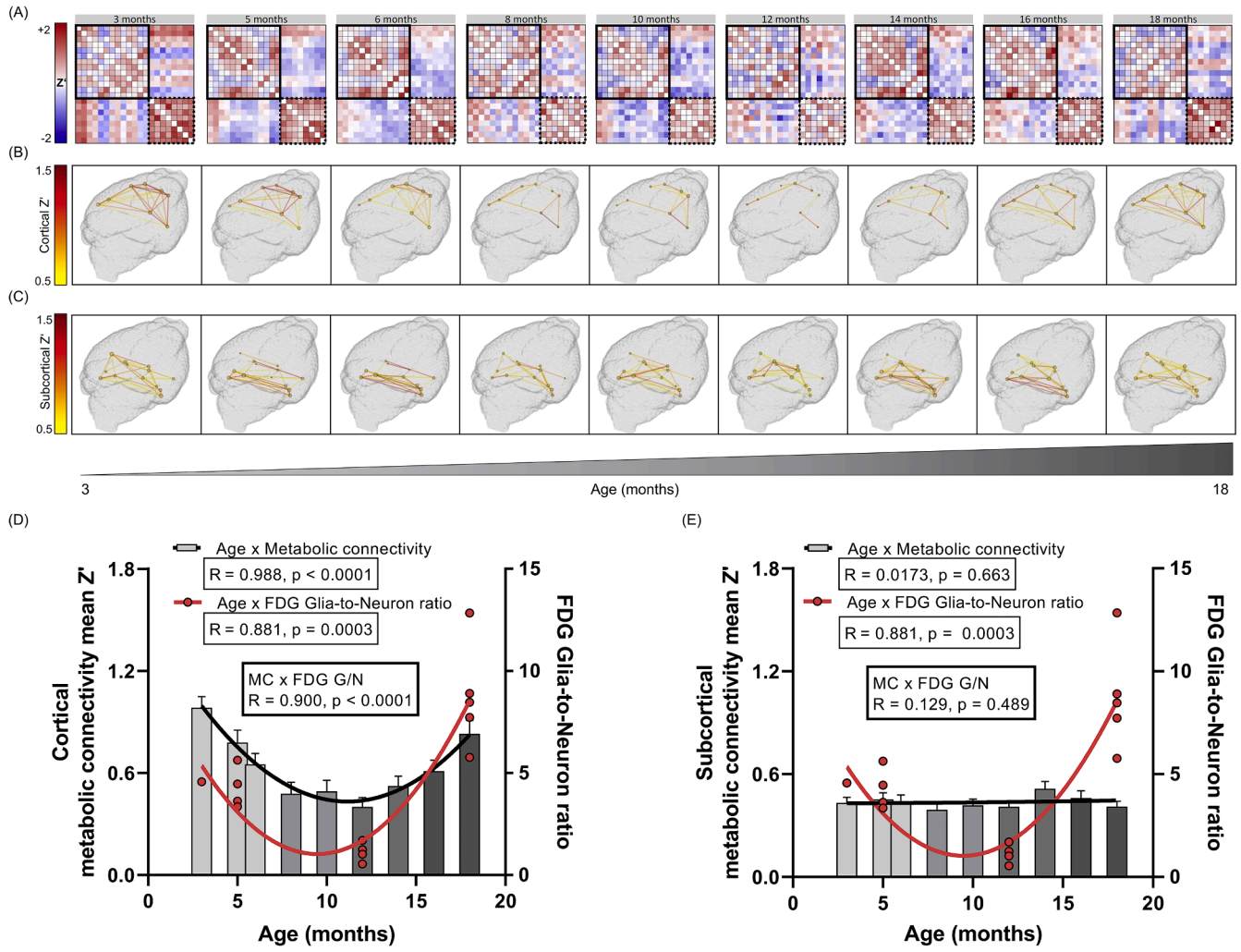

Fig. 2. Metabolic connectivity and its association with the FDG Glia-to-Neuron-ratio during aging in wild-type mice. (A) Single boxes indicate inter-regional Z' as an index of metabolic connectivity between each pair of brain regions (subcortical: black lines, cortical: black dots). Connections of hubs projected upon a 3D mouse brain template show significant intra-correlation-coefficients for cortical and subcortical brain networks over time. (B) Mean intra-correlation-coefficients as a function of age (black) for cortical and subcortical networks in correlation with FDG Glia-to-Neuron-ratios as a function of age (red).

terms of translation, we note that abundance of neurons and astroglial cells varies across species (Herculano-Houzel, 2009; Herculano-Houzel, 2014) and that aged mice may not reflect the aged human brain (Brendel et al., 2017). Furthermore, scRadiotracing only allows isolation of cellular bodies, as processes and axons are lost during brain dissociation. Therefore, absolute cellular FDG uptake of neurons and astrocytes will be underestimated since FDG is also located in synapses and processes. However, under the assumption that synapses and processes are equally lost at different ages, temporal changes in FDG uptake per cell can still be reliably modelled against temporal changes in FDG-PET signals (Gnörich et al., 2023). For the first time, this approach allowed to estimate detailed allocation of cell type contributions to FDG-PET signals at different ages in mice. The estimated proportions of 53 %−89 % astroglial contribution to the overall FDG uptake in the mouse brain matched with studies that claimed ~85 % brain-wide glucose consumption of astrocytes (Ryu et al., 2021). As an interesting observation, the parabolic course of cortical metabolic connectivity during aging in mice was closely matched with proportions of cellular glucose uptake in astroglia and neurons (i.e. the FDG Glia-to-Neuron-ratio). In the broader context, the Glia-to-Neuron-ratio serves as an indicator of the proportion between the total count of glial cells and neurons within a structure, regardless of their respective sizes. Moreover, it is a commonly employed metric in the field of biological research (von Bartheld et al., 2016). The current data highlights a consistent pattern of cellular glucose uptake per individual cell in astrocytes and microglia, aligning with previous findings that indicate the activation of both cell types during the late aging process (Palmer and Ousman, 2018; Antignano et al., 2023). Our finding is in line with decreased metabolic connectivity upon depletion of microglia and increases of metabolic connectivity in a mouse model with hyperactive microglia (Gnörich et al., 2023). Consistent with our earlier investigation revealing no notable variations in subcortical metabolic connectivity among distinct mouse models with diverging microglial phenotypes (Gnörich et al., 2023), the current study did not identify any significant alterations in subcortical networks during aging. We hypothesize that the cortex undergoes more pronounced age-related changes, including reductions in neuronal density and synaptic connections, which, along with glial immune cell activation, may contribute to alterations in metabolic connectivity (Albertson et al., 2022; Allen et al., 2023). In contrast, subcortical structures in rodents are poorly classified and exhibit heterogeneity in terms of neuronal density (Keller et al., 2018). We assume that subcortical regions may experience less significant changes in cellular composition with aging, maintaining relatively balanced levels of neurons and glial cells. However, while these subcortical regions are still susceptible to age-related functional changes, their cellular composition and metabolic signature may be less affected compared to the cortex.

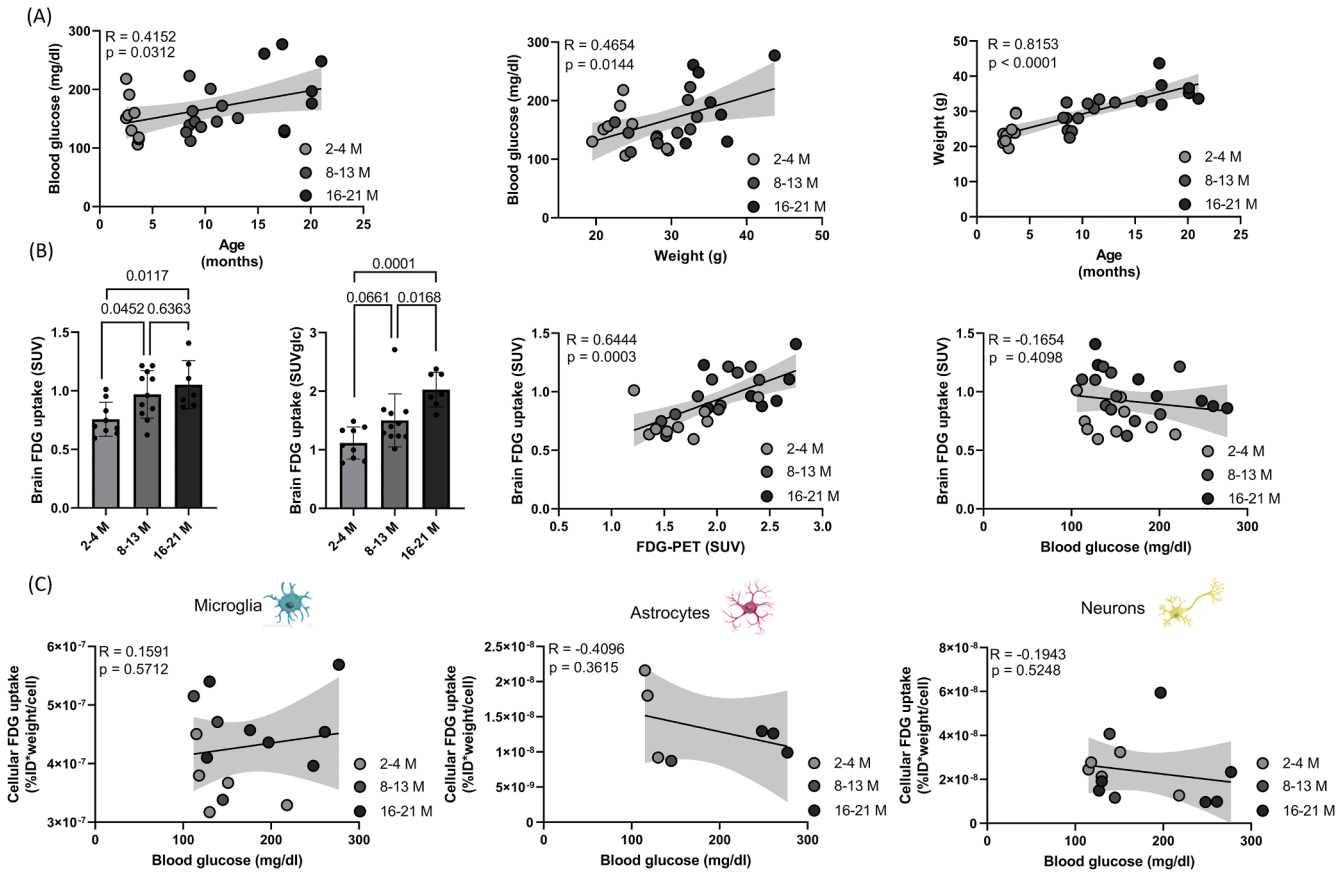

Fig. 3. Associations between blood glucose levels and FDG uptake in brain and single cells during aging. (A) Associations between blood glucose levels, age and weight. (B) Whole brain activity in comparison of three ages (2–4/8–13/17–21 months), normalized by SUV and corrected for blood glucose levels (SUVglc). Associations between blood glucose levels. brain FDG uptake and whole brain FDG-PET uptake. (C) Associations between blood glucose levels and single cell FDG uptake of microglia, astrocytes and neurons, normalized by injected dose and body weight.

Interestingly, the interregional cortico-hippocampal network decreased as a logarithmic function of age, most likely as a consequence of a multifactorial process, driven by a combination of cellular, molecular, and systemic changes. One of the most direct consequences of aging is neuronal loss and atrophy in both the hippocampus and cortex of humans and mice (Bettio et al., 2017; Radulescu et al., 2021). This neuronal loss is often accompanied by a decrease in dendritic complexity and spine density, further impairing the communication between these regions (Calì et al., 2018). In human brains, hippocampus shrinkage increased and accelerated with age compared to other brain regions (Raz et al., 2005; Bishop et al., 2010). Furthermore, inflammation can impair synaptic function and disrupt neurogenesis, particularly in the hippocampus (Barrientos et al., 2015). The release of pro-inflammatory cytokines and other inflammatory mediators can lead to synaptic pruning, neuronal death, and a reduction in synaptic plasticity, all of which potentially contribute to decreased metabolic connectivity during aging (Rosenzweig and Barnes, 2003). Subregional application of our novel scRadiotracing approach could provide deeper insights into the differences in intra- and interregional metabolic networks. Additionally, the investigation of glutamate transporter (Zimmer et al., 2017) and glucose transporter 1 (Koepsell, 2020) expression across cortical and subcortical regions could be effectively assessed using immunohistochemistry and sequencing techniques. The use of novel spatial transcriptomics techniques could also facilitate the spatial alignment of molecular imaging data, such as glucose metabolism imaging and metabolic connectome analyses (Zheng et al., 2023). Collectively, these approaches would allow for a more comprehensive analysis of the underlying biology within a spatial context, enabling the detailed mapping of cellular networks, identification of cell types, and a better understanding of the spatial interactions between different molecules.

Of note, neurons showed highest cellular FDG uptake at 10–13 months of age. These results are in line with previous findings suggesting neuronal hyperacitivity during healthy aging, with highest neuronal excitability from 10 months of age (Lerdkrai et al., 2018). The decrease of neuronal FDG uptake at the old age may be result of reduced neuroplasticity and loss of synaptic function, which also occur in the healthy aging brain (Bishop et al., 2010). Future studies could shed light on distinct glucose uptake of excitatory vs. inhibitory neurons during healthy aging, using specific antibodies such as VGLUT1 (Fremeau et al., 2004) and GAD1/67 (Chattopadhyaya et al., 2007).

We acknowledge that the large cohort of wild-type mice scanned with the Inveon system presents with relatively low whole brain SUV compared to other published reports in awake mice e.g. (Welch et al., 2013) and compared to the second cohort scanned with the Medisosystem. The latter comparison suggests an impact of sensitivity and resolution, whereas anesthesia is also known to account for lower brain FDG uptake in brain (Shimoji et al., 2004; Fueger et al., 2006; Gnörich et al., 2024). Nevertheless, to prioritize animal welfare, we omitted to conduct the experiments in an awake state, since our previous studies indicated robust effects between genotypes for PET and cell uptake measures (Xiang et al., 2021; Gnörich et al., 2023) as well as for metabolic connectivity read outs (Ruch et al., 2024) in consideration of awake and anesthesized states. In this regard, cellular FDG uptake between neurons, astrocytes and microglia was equal for injection during isoflurane anesthesia versus awake injection and proportional to the applied dose of FDG (Xiang et al., 2021).

Since brain PET signals comprise a product of cellular tracer uptake and cellular abundance, proliferation of cells directly influences the

relative proportions of FDG allocation in the brain. We extensively explored this phenomenon in the context of TSPO-PET imaging for glioblastoma (Bartos et al., 2023) and observed that the PET signal from tumors could be effectively explained by the additive contribution of tumor and immune cells. Unlike TSPO, which is located at the outer mitochondrial membrane within the cell soma, detecting the entire FDG uptake of individual cells is unattainable due to the loss of processes and synapses during cell sorting. We thoroughly discussed this limitation in a technical comment appended to a previously published paper (Xiang et al., 2021). Nevertheless, our previous investigations revealed that alterations in FDG uptake of cell bodies accurately reflecte cell type related changes (Gnörich et al., 2023). Consequently, our present findings characterize relative changes within a specific cell population over time but cannot be used for direct calculation of absolute FDG allocation to different cell types under consideration of their abundance. Nonetheless, the applied equation system enabled us to estimate the contributions of each cell type population to the FDG-PET signal at different age stages. In this analysis, we accounted for the proliferation of microglia, astrocytes, and neurons over time, utilizing previously published estimations of cell type-specific numbers in the aging mouse brain (Askew et al., 2017; Deng et al., 2006). These data indicated a 14 % increase in microglia cells in aged mice but did not suggest substantial changes in the abundance of neurons and astrocytes. Given the discrepancies between in vitro FDG uptake assays (Cossu et al., 2019) and the obtained in vivo snap shot of cellular FDG uptake by scRadiotracing, future studies shoud aim for head-to-head comparisons. Also, the methodological approach of cell sorting after FDG injection presented in this study can be used to furthermore disentangle the contributions of additional stromal cells such as e.g. oligodentrocytes, endothelial cells and lymphocytes to FDG-PET signals during aging.

Besides the pons and the global mean, the use of the cerebellum and brainstem as reference regions in FDG-PET SUVR studies is well-established in literature, providing weight-independet indices for FDG uptake (Nugent et al., 2020; Li et al., 2016). Our group previously demonstrated an inverted parabolic trajectory in FDG-PET SUVR in longitudinally assessed wild-type mice, with levels increasing until 14.5 months and subsequently declining by 20 months of age (Brendel et al., 2017). However, data on the cellular composition of FDG-PET signals in reference and target subregions are currently lacking. Our current study offers comprehensive insights into the impact of astroglia on FDG-PET signals, particularly in the elderly mouse brain. Combined consideration of our whole-brain SUV findings with previous SUVR data, may allow the conclusion that the observed relative decline in cortical glucose metabolism in elderly wild-type mice is attributed to a relatively lower contribution of microglial FDG uptake in the cortex compared to the cerebellum and brainstem. Nevertheless, further studies are needed to investigate region-specific FDG uptake at the cellular level.

We also acknowledge the disparity between the number of female and male mice included in this study, which limits our ability to account for sex differences. Recent studies highlighted the significant role of glial cells, in brain aging and neuroinflammation, with emerging evidence pointing to sex-specific differences in their metabolic responses (Ibrahim et al., 2020; Crespo-Castrillo and Arevalo, 2020). For instance, rodent microglia exhibited sex-specific metabolic responses indicating that male microglia may be more prone to shifting towards pro-inflammatory state in the early developing brain. Conversely, increased microglial activation in females during adulthood could contribute to their heightened vulnerability to various inflammatory brain diseases that manifest later in life (Han et al., 2021). Studies using FDG-PET have reported sex differences in brain metabolism among healthy participants (Feng et al., 2022) and in Alzheimer's disease (Park et al., 2023). Similarly, TSPO-PET binding, as a surrogate for microglial activity, has been associated with sex in both humans (Tuisku et al., 2019) and rodents (Biechele et al., 2020), indicating sex-dependent variations in microglial activation with aging. Based on these data, we hypothesize that the glia-to-neuron ratio will become more pronounced in females compared to males in the later stages of aging, potentially altering metabolic connectivity.

In a subset of mice, we intended to investigate the relationship between blood glucose levels, body weight, brain FDG uptake and cellular FDG uptake. The observed linear increase in blood glucose levels and body weight as a function of age aligns with previous findings in wild-type mice until the age of 19 months (Petr et al., 2021). Subsequently, FDG-PET and ex vivo brain FDG uptake were adjusted for blood glucose levels to obtain a surrogate for the metabolic rate of glucose (Bertoglio et al., 2021), but age related increases in both indices were still present. Furthermore, we did not find a direct association between blood glucose levels and cell specific FDG uptake in microglia, astrocytes, and neurons. Together these findings suggest that blood glucose is not a driver of age-related increases in cerebral FDG-PET signals.

In summary, our findings provide insights into the complex interplay of blood glucose levels, body weight, age-related changes in cellular FDG uptake and metabolic connectivity of cerebral FDG-PET signals. The observed associations underscore the importance of considering multiple factors in the interpretation of FDG-PET data to understand age-related alterations in brain metabolism. Although neurons may have a stronger contribution to FDG uptake in the human brain compared to rodents (Herculano-Houzel, 2009), astroglia should be considered as an influencer of metabolic connectivity assessment (S. Morbelli et al., 2013) in future studies. This could be especially relevant in early disease stages of AD, where FDG-PET hypermetabolism was already linked to biomarkers of microglial activation (Biel et al., 2023).

Ethics approval

The experiments have been approved by the local animal care committee of the Government of Oberbayern (Regierung Oberbayern), overseen by a veterinarian and in compliance with the ARRIVE guidelines and were carried out in accordance with the U.K. Animals (Scientifc Procedures) Act, 1986 and associated guidelines, EU Directive 2010/63/EU for animal experiments.

Funding

This work was supported by grants from the Deutsche Forschungsgemeinschaft (DFG, German Research Foundation) under Germany's Excellence Strategy within the framework of the Munich Cluster for Systems Neurology (EXC 2145 SyNergy—ID 390857198). S.T. was supported by the Alzheimer Forschung Initiative e.V. (Grant Number 18014).

CRediT authorship contribution statement

Laura M. Bartos: Writing – original draft, Visualization, Validation, Software, Resources, Methodology, Investigation, Formal analysis, Data curation, Conceptualization. **Sebastian T. Kunte:** Resources, Methodology, Investigation, Data curation. **Stephan Wagner:** Methodology, Data curation. **Philipp Beumers:** Resources, Methodology, Investigation, Data curation. **Rebecca Schaefer:** Resources, Methodology, Investigation, Data curation. **Artem Zatcepin:** Software, Resources, Methodology. **Yunlei Li:** Methodology, Data curation. **Maria Griessl:** Software, Methodology. **Leonie Hoermann:** Resources, Methodology, Investigation, Data curation. **Karin Wind-Mark:** Supervision, Resources, Methodology. **Peter Bartenstein:** Writing – review & editing, Supervision, Software. **Sabina Tahirovic:** Writing – review & editing, Supervision, Software. **Sibylle Ziegler:** Writing – review & editing, Supervision, Software. **Matthias Brendel:** Writing – review & editing, Visualization, Supervision, Software, Project administration, Funding acquisition, Formal analysis, Conceptualization. **Johannes Gnörich:** Writing – review & editing, Visualization, Validation, Supervision, Resources, Project administration, Methodology, Investigation, Formal analysis, Data curation, Conceptualization.

Declaration of competing interest

MB is a member of the Neuroimaging Committee of the EANM. MB received speaker honoraria from Roche, GE healthcare and Life Molecular Imaging, has advised Life Molecular Imaging and is currently in the advisory board of MIAC. All other authors do not report any conflict of interest.

Data availability

The datasets generated during and/or analysed during the current study are available from the corresponding author on reasonable request.

Acknowledgements

We thank Rosel Oos and Giovanna Palumbo for excellent technical support during PET imaging.

Supplementary materials

Supplementary material associated with this article can be found, in the online version, at doi:10.1016/j.neuroimage.2024.120860.

References

Albertson, A.J., et al., 2022. Normal aging in mice is associated with a global reduction in cortical spectral power and network-specific declines in functional connectivity. Neuroimage 257, 119287.
Allen, W.E., et al., 2023. Molecular and spatial signatures of mouse brain aging at single-cell resolution. Cell 186 (1), 194–208 e18.
Antignano, I., et al., 2023. Aging microglia. Cell. Mol. Life Sci. 80 (5), 126.
Askew, K., et al., 2017. Coupled proliferation and apoptosis maintain the rapid turnover of microglia in the adult brain. Cell Rep. 18 (2), 391–405.
Barrientos, R.M., et al., 2015. Neuroinflammation in the normal aging hippocampus. Neuroscience 309, 84–99.
Bartos, L.M., et al., 2022. Single-cell radiotracer allocation via immunomagnetic sorting to disentangle PET signals at cellular resolution. J. Nucl. Med. 63 (10), 1459–1462.
Bartos, L.M., et al., 2023. Deciphering sources of PET signals in the tumor microenvironment of glioblastoma at cellular resolution. Sci. Adv. 9 (43), eadi8986.
Bertoglio, D., et al., 2021. Estimation of the net influx rate Ki and the cerebral metabolic rate of glucose MRglc using a single static [18F]FDG PET scan in rats. Neuroimage 233, 117961.
Bettio, L.E.B., Rajendran, L., Gil-Mohapel, J., 2017. The effects of aging in the hippocampus and cognitive decline. Neurosci. Biobehav. Rev. 79, 66–86.
Biechele, G., et al., 2020. Glial activation is moderated by sex in response to amyloidosis but not to tau pathology in mouse models of neurodegenerative diseases. J. Neuroinflammation 17 (1), 374.
Biel, D., et al., 2023. sTREM2 is associated with amyloid-related p-tau increases and glucose hypermetabolism in Alzheimer's disease. EMBO Mol. Med. 15 (2), e16987.
Bishop, N.A., Lu, T., Yankner, B.A., 2010. Neural mechanisms of ageing and cognitive decline. Nature 464 (7288), 529–535.
Bohnen, N.I., et al., 2012. Effectiveness and safety of 18F-FDG PET in the evaluation of dementia: a review of the recent literature. J. Nucl. Med. 53 (1), 59–71.
Brendel, M., et al., 2016. Glial activation and glucose metabolism in a transgenic amyloid mouse model: a triple-tracer PET study. J. Nucl. Med. 57 (6), 954–960.
Brendel, M., et al., 2017. Time courses of cortical glucose metabolism and microglial activity across the life span of wild-type mice: a PET study. J. Nucl. Med. 58 (12), 1984–1990.
Calì, C., et al., 2018. The effects of aging on neuropil structure in mouse somatosensory cortex—a 3D electron microscopy analysis of layer 1. PLoS ONE 13 (7), e0198131.
Chattopadhyaya, B., et al., 2007. GAD67-mediated GABA synthesis and signaling regulate inhibitory synaptic innervation in the visual cortex. Neuron 54 (6), 889–903.
Cossu, V., et al., 2019. Obligatory role of endoplasmic reticulum in brain FDG uptake. Eur. J. Nucl. Med. Mol. Imaging 46 (5), 1184–1196.
Crespo-Castrillo, A., Arevalo, M.A., 2020. Microglial and astrocytic function in physiological and pathological conditions: estrogenic modulation. Int. J. Mol. Sci. 21 (9).
de Cristobal, J., et al., 2014. Longitudinal assessment of a transgenic animal model of tauopathy by FDG-PET imaging. J. Alzheimers Dis. 40 (Suppl 1), S79–S89.
Deng, X.H., et al., 2006. Cytokine-induced activation of glial cells in the mouse brain is enhanced at an advanced age. Neuroscience 141 (2), 645–661.
Feng, B., et al., 2022. Gender-related differences in regional cerebral glucose metabolism in normal aging brain. Front. Aging Neurosci. 14, 809767.
Focke, C., et al., 2019. Early and longitudinal microglial activation but not amyloid accumulation predicts cognitive outcome in PS2APP mice. J. Nucl. Med. 60 (4), 548–554.
Fremeau Jr., R.T., et al., 2004. VGLUTs define subsets of excitatory neurons and suggest novel roles for glutamate. Trends Neurosci. 27 (2), 98–103.
Fueger, B.J., et al., 2006. Impact of animal handling on the results of ^{18}F-FDG PET studies in mice. J. Nucl. Med. 47 (6), 999–1006.
Gnörich, J., et al., 2023. Depletion and activation of microglia impact metabolic connectivity of the mouse brain. J. Neuroinflammation 20 (1), 47.
Gnörich, J., et al., 2024. Towards multicenter β-amyloid PET imaging in mouse models: a triple scanner head-to-head comparison. Neuroimage 297, 120748.
Han, J., et al., 2021. Uncovering sex differences of rodent microglia. J Neuroinflammation 18 (1), 74.
Herculano-Houzel, S., 2009. The human brain in numbers: a linearly scaled-up primate brain. Front. Hum. Neurosci. 3, 31.
Herculano-Houzel, S., 2014. The glia/neuron ratio: how it varies uniformly across brain structures and species and what that means for brain physiology and evolution. Glia 62 (9), 1377–1391.
Ibrahim, M.M.H., et al., 2020. Sex-specific estrogen regulation of hypothalamic astrocyte estrogen receptor expression and glycogen metabolism in rats. Mol. Cell. Endocrinol. 504, 110703.
Kakimoto, A., et al., 2016. Age-related sex-specific changes in brain metabolism and morphology. J. Nucl. Med. 57 (2), 221–225.
Kalpouzos, G., et al., 2009. Voxel-based mapping of brain gray matter volume and glucose metabolism profiles in normal aging. Neurobiol. Aging 30 (1), 112–124.
Keller, D., Erö, C., Markram, H., 2018. Cell densities in the mouse brain: a systematic review. Front. Neuroanat 12.
Koepsell, H., 2020. Glucose transporters in brain in health and disease. Pflügers Archiv - Eur. J. Physiol. 472 (9), 1299–1343.
Lerdkrai, C., et al., 2018. Intracellular Ca(2+) stores control in vivo neuronal hyperactivity in a mouse model of Alzheimer's disease. Proc. Natl. Acad. Sci. U. S. A. 115 (6), E1279–E1288.
Li, X.Y., et al., 2016. Age- and brain region-specific changes of glucose metabolic disorder, learning, and memory dysfunction in early Alzheimer's disease assessed in APP/PS1 transgenic mice using (18)F-FDG-PET. Int. J. Mol. Sci. 17 (10).
Ma, Y., et al., 2005. A three-dimensional digital atlas database of the adult C57BL/6J mouse brain by magnetic resonance microscopy. Neuroscience 135 (4), 1203–1215.
Morbelli, S., et al., 2013a. Metabolic networks underlying cognitive reserve in prodromal alzheimer disease: a European alzheimer disease consortium project. J. Nucl. Med. 54 (6), 894–902.
Morbelli, S., et al., Metabolic networks underlying cognitive reserve in prodromal Alzheimer disease: a European Alzheimer disease consortium project. 2013. 54(6): p. 894–902.
Nugent, S., et al., 2020. Selection of the optimal intensity normalization region for FDG-PET studies of normal aging and Alzheimer's disease. Sci Rep 10 (1), 9261.
Palmer, A.L., Ousman, S.S., 2018. Astrocytes and Aging. Front. Aging Neurosci. 10.
Park, J.-C., et al., 2023. Sex differences in the progression of glucose metabolism dysfunction in Alzheimer's disease. Exp. Mol. Med. 55 (5), 1023–1032.
Petr, M.A., et al., 2021. A cross-sectional study of functional and metabolic changes during aging through the lifespan in male mice. Elife 10, e62952.
Poisnel, G., et al., 2012. Increased regional cerebral glucose uptake in an APP/PS1 model of Alzheimer's disease. Neurobiol. Aging 33 (9), 1995–2005.
Radulescu, C.I., et al., 2021. The aging mouse brain: cognition, connectivity and calcium. Cell Calcium 94, 102358.
Raz, N., et al., 2005. Regional brain changes in aging healthy adults: general trends, individual differences and modifiers. Cereb. Cortex 15 (11), 1676–1689.
Rocha, A., et al., 2022. Clozapine induces astrocyte-dependent FDG-PET hypometabolism. Eur. J. Nucl. Med. Mol. Imaging 49 (7), 2251–2264.
Rosenzweig, E.S., Barnes, C.A., 2003. Impact of aging on hippocampal function: plasticity, network dynamics, and cognition. Prog. Neurobiol. 69 (3), 143–179.
Ruch, F., et al., 2024. Validity and value of metabolic connectivity in mouse models of β-amyloid and tauopathy. Neuroimage 286, 120513.
Ryu, W.-I., et al., 2021. Brain cells derived from Alzheimer's disease patients have multiple specific innate abnormalities in energy metabolism. Mol. Psychiatry 26 (10), 5702–5714.
Shimoji, K., et al., 2004. Measurement of cerebral glucose metabolic rates in the anesthetized rat by dynamic scanning with ^{18}F-FDG, the ATLAS small animal PET scanner, and arterial blood sampling. J. Nucl. Med. 45 (4), 665–672.
Tuisku, J., et al., 2019. Effects of age, BMI and sex on the glial cell marker TSPO — A multicentre [11C]PBR28 HRRT PET study. Eur. J. Nucl. Med. Mol. Imaging 46 (11), 2329–2338.
von Bartheld, C.S., Bahney, J., Herculano-Houzel, S., 2016. The search for true numbers of neurons and glial cells in the human brain: a review of 150 years of cell counting. J. Comp. Neurol. 524 (18), 3865–3895.
Welch, A., et al., 2013. Mapping changes in mouse brain metabolism with PET/CT. J. Nucl. Med. 54 (11), 1946–1953.
Xiang, X., et al., 2021. Microglial activation states drive glucose uptake and FDG-PET alterations in neurodegenerative diseases. Sci. Transl. Med. 13 (615), eabe5640.
Zheng, P., et al., 2023. Integrated spatial transcriptome and metabolism study reveals metabolic heterogeneity in human injured brain. Cell Rep. Med. 4 (6), 101057.
Zimmer, E.R., et al., 2017. [(18)F]FDG PET signal is driven by astroglial glutamate transport. Nat. Neurosci. 20 (3), 393–395.